J. Fluid Mech. (2000), *vol.* 416, *pp.* 29–43. Printed in the United Kingdom

Stability of elliptical horizontally inhomogeneous rodons

By RENÉ PINET[1]† AND E. G. PAVÍA[2]

[1]Universidad Autónoma de Baja California, México
[2]Centro de Investigación Científica y de Educación Superior de Ensenada, México

(Received 30 July 1999 and in revised form 15 February 2000)

The stability of one-layer vortices with inhomogeneous horizontal density distributions is examined both analitically and numerically. Attention is focused on elliptical vortices for which the formal stability theorem proved by Ochoa, Sheinbaum & Pavía (1988) does not apply. Our method closely follows that of Ripa (1987) developed for the homogeneous case; and indeed they yield the same results when inhomogenities vanish. It is shown that a criterion from the formal analysis – the necessity of a radial increase in density for instability – does not extend to elliptical vortices. In addition, a detailed examination of the evolution of the inhomogeneous density fields, provided by numerical simulations, shows that homogenization, axisymmetrization and loss of mass to the surroundings are the main effects of instability.

1. Introduction

In a recent paper Ochoa, Sheinbaum & Pavía (1988), using a one-layer reduced-gravity model with variable density, established a procedure to generate families of solutions with the same flow structure as any non-divergent solution of the classical homogeneous vortex model. These so-called inhomogeneous rodons were constructed as explicit examples of exact solutions on the f-plane, and their formal stability (Holm *et al.* 1985) was studied. A theorem, valid for circular vortices, showed that in order to be unstable the density of the inhomogeneous rodon must increase outward somewhere. Furthermore, some numerical simulations performed by the same authors (Ochoa *et al.* 1998) suggested that this formal stability theorem might be applicable to non-circular inhomogeneous rodons as well. In this work we rework the analytical study of the stability of elliptical inhomogeneous rodons in a normal modes fashion, since the formal stability method is prohibited for this non-circular case. Moreover, we complement the stability study with numerical simulations to illustrate the details of the vortex evolution.

We begin by briefly presenting the model first proposed by Schopf & Cane (1983) which includes, in an approximate manner, the effects of density inhomogeneity. For just one active layer the model is better cast, as shown by Ripa (1996), in terms of the fields $\gamma = \theta^{1/2}$ and $\phi = \theta^{1/2}h$, where $\theta(\boldsymbol{r}, t) = g(\bar{\rho} - \rho(\boldsymbol{r}, t))/\bar{\rho}$ is the buoyancy (which is required to be non-negative definite), g is gravity, ρ is the (space- and time-dependent) mass density of the active layer, $\bar{\rho}$ is the uniform mass density of the inert lower layer, $h = h(\boldsymbol{r}, t)$ is the thickness of the active layer, $\boldsymbol{r}$ is the horizontal vector position, and

† Present address: Facultad de Ciencias Marinas, UABC. Unidad Universitaria Ensenada, Baja California 22800, México. e-mail: rpinet@bahia.ens.uabc.mx.

t is time. The equations are

$$\frac{\partial \phi}{\partial t} + \nabla \cdot (\phi \boldsymbol{u}) = 0, \tag{1.1a}$$

$$\frac{\partial \boldsymbol{u}}{\partial t} + \boldsymbol{u} \cdot \nabla \boldsymbol{u} + f \hat{\boldsymbol{k}} \times \boldsymbol{u} + \gamma \nabla \phi = 0, \tag{1.1b}$$

$$\frac{\partial \gamma}{\partial t} + \boldsymbol{u} \cdot \nabla \gamma = 0, \tag{1.1c}$$

where $\boldsymbol{u}$ is the horizontal velocity and f is the Coriolis parameter; $\hat{\boldsymbol{k}}$ is the unit vertical (in the opposite direction to gravity) vector.

2. Base solutions

Ripa (1996) and Ochoa *et al.* (1998) have proposed ways to obtain base solutions for the inhomogeneous system (1.1), from solutions to the homogeneous problem

$$\frac{\mathrm{D}\hat{h}}{\mathrm{D}t} + \hat{h} \nabla \cdot \boldsymbol{u} = 0, \tag{2.1a}$$

$$\frac{\mathrm{D}\boldsymbol{u}}{\mathrm{D}t} + f \hat{\boldsymbol{k}} \times \boldsymbol{u} + \hat{g} \nabla \hat{h} = 0, \tag{2.1b}$$

where $\hat{g}$ is the (constant) reduced gravity. It is convenient to distinguish between the active layer depth for the homogeneous problem ($\hat{h}$) and that for the inhomogeneous problem (h).

If, for a solution to (2.1a)

$$\frac{\mathrm{D}\hat{h}}{\mathrm{D}t} = 0,$$

i.e. the velocity field is non-divergent, then γ and ϕ can be represented as depending on $\hat{h}$ only, satisfying

$$\gamma(\hat{h})\, \mathrm{d}\phi = \hat{g}\, \mathrm{d}\hat{h}, \tag{2.2}$$

since

$$\frac{\mathrm{D}\gamma}{\mathrm{D}t} = \frac{\mathrm{d}\gamma}{\mathrm{d}\hat{h}} \frac{\mathrm{d}\hat{h}}{\mathrm{d}t}, \quad \frac{\mathrm{D}\phi}{\mathrm{D}t} = \frac{\mathrm{d}\phi}{\mathrm{d}\hat{h}} \frac{\mathrm{d}\hat{h}}{\mathrm{d}t}.$$

Systems (1.1) and (2.1) have, then, the same velocity field $\boldsymbol{u}$ as a solution. Of course, the active layer depth of the inhomogeneous rodon is

$$h(\hat{h}) = \frac{\phi(\hat{h})}{\gamma(\hat{h})}, \tag{2.3}$$

and the role of $\hat{h}$ has been reduced to that of an internal variable used to describe the radial distribution of properties.

Now, for elliptical vortices, Ripa (1987) found it useful to introduce the f_*-plane

$$(x_* + \mathrm{i}y_*) = (x + \mathrm{i}y)\mathrm{e}^{\mathrm{i}\Omega t}, \tag{2.4}$$

and $f_* = f - 2\Omega$, where Ω is the rotation rate of the frontal ellipse or the 'vortex precession', and

$$\Omega_* = [\Omega(f - \Omega)]^{1/2}. \tag{2.5}$$

The function $\boldsymbol{u}_* = (u_*, v_*)$ can be defined for $\boldsymbol{r}_* = (x_*, y_*)$:

$$\boldsymbol{u}_*(r_*, t) = (u_*, v_*) = \boldsymbol{u}(r, t) \circ r(r_*).$$

From this point on all work will be carried out in the f_*-plane, and scalar fields $\hat{h}, \phi, \psi$ will be appropriately redefined as†

$$\left.\begin{matrix} \hat{h}(\boldsymbol{r}_*, t) \\ \phi(\boldsymbol{r}_*, t) \\ \psi(\boldsymbol{r}_*, t) \end{matrix}\right\} := \left\{\begin{matrix} \hat{h}(\boldsymbol{r}, t) \\ \phi(\boldsymbol{r}, t) \\ \psi(\boldsymbol{r}, t) \end{matrix}\right\} \circ \boldsymbol{r}(\boldsymbol{r}_*, t),$$

or even, as it has been done in (2.3),

$$\left.\begin{matrix} \phi(\hat{h}, t) \\ \psi(\hat{h}, t) \end{matrix}\right\} := \left.\begin{matrix} \phi(\boldsymbol{r}, t) \\ \psi(\boldsymbol{r}, t) \end{matrix}\right\} \circ \boldsymbol{r}(\boldsymbol{r}_*, t) \circ \boldsymbol{r}_*(\hat{h}).$$

Equations (2.1) in the f_*-plane are

$$\frac{\mathrm{D}\hat{h}}{\mathrm{D}t} + \hat{h}\nabla \cdot \boldsymbol{u}_* = 0,$$

$$\frac{\mathrm{D}\boldsymbol{u}_*}{\mathrm{D}t} + f_* \hat{\boldsymbol{k}} \times \boldsymbol{u}_* + \hat{g}\nabla\hat{h} + \Omega_*^2 \boldsymbol{r}_* = 0,$$

and system (1.1) becomes

$$\frac{\partial \phi}{\partial t} + \nabla \cdot (\phi \boldsymbol{u}_*) = 0, \tag{2.6a}$$

$$\frac{\partial \boldsymbol{u}_*}{\partial t} + \boldsymbol{u}_* \cdot \nabla \boldsymbol{u}_* + f_* \hat{\boldsymbol{k}} \times \boldsymbol{u}_* + \gamma \nabla \phi + \Omega_*^2 \boldsymbol{r}_* = 0, \tag{2.6b}$$

$$\frac{\partial \gamma}{\partial t} + \boldsymbol{u}_* \cdot \nabla \gamma = 0. \tag{2.6c}$$

If a and b are the ellipse's semi-axes, then

$$\hat{h}(\boldsymbol{r}_*, t) = \frac{a\,b}{2\,\hat{g}}\,\Omega_*\,f_*\left(1 - \left(\frac{x_*}{a}\right)^2 - \left(\frac{y_*}{b}\right)^2\right); \tag{2.7}$$

its value at the vortex centre is denoted as $\hat{h}_m = \hat{h}|_{x_*=0, y_*=0}$.

From (2.3), we can choose an arbitrary density distribution function $\phi_0(\hat{h})$, and obtain $\gamma_0(\hat{h})$:

$$\gamma_0(\hat{h}) = \frac{\hat{g}}{\mathrm{d}\phi_0/\mathrm{d}\hat{h}}, \tag{2.8}$$

using, as in Ochoa *et al.* (1998),

$$\phi_0(\hat{h}) = \hat{h}\hat{g}^{1/2}\left(1 + \frac{\mu}{2}\frac{\hat{h}}{\hat{h}_m}\right), \tag{2.9}$$

where μ is a parameter which controls the inhomogeneity.

This implies

$$\gamma_0(\hat{h}) = \frac{\hat{g}^{1/2}}{1 + \mu\hat{h}/\hat{h}_m}, \tag{2.10}$$

† Extended notation is used for composition of functions $f \circ g(x)$, defined as $f(g(x))$.

and an active layer depth profile

$$h(\hat{h}) = \hat{h}(1 + \mu\hat{h}/\hat{h}_m)\left(1 + \frac{\mu}{2}\hat{h}/\hat{h}_m\right). \tag{2.11}$$

3. Method

A non-divergent solution for the homogeneous case has the same flow structure in the homogeneous and inhomogeneous cases, as has been described in § 2. For the inhomogeneous case, therefore, a non-divergent inhomogeneous rodon is set as the basic solution. The two horizontal components of velocity are the same as in the homogeneous case:

$$u_0 = (a\,\Omega_* y_*)/b, \qquad v_0 = -(b\,\Omega_* x_*)/a. \tag{3.1}$$

The depth and density fields, represented through variables $\phi := \hat{h}\,\theta^{1/2}(\hat{h})$ and $\psi := 1/\gamma(\hat{h}) = \theta^{-1/2}(\hat{h})$, will be taken from the inhomogeneous rodon solution as obtained by Ochoa *et al.* (1998):

$$\phi_0(\hat{h}) = \hat{h}\left(1 + \frac{\mu}{2}\frac{\hat{h}}{\hat{h}_m}\right)\hat{g}^{1/2}, \tag{3.2}$$

$$\psi_0(\hat{h}) = \left(1 + \mu\frac{\hat{h}}{\hat{h}_m}\right)\hat{g}^{-1/2}, \tag{3.3}$$

where $\hat{h}$ (the layer thickness) and $\hat{g}$ (the reduced gravity) have lost, in the inhomogeneous case, their physical meaning; they remain only as parameters for radial position and horizontal density distribution, respectively. Constant parameter $\hat{h}_m = ab\Omega_* f_*/(2\hat{g})$ is the maximum value of $\hat{h}(\boldsymbol{r}_*)$ at the initial time. Note that the layer thickness in the inhomogeneous case $h = \phi/\gamma$ coincides with or is directly proportional to $\hat{h}$ only when γ is uniform.

For elliptical vortices, our stability analysis follows closely that of Ripa (1987) for homogeneous rodons. While Ripa (1987) and Ochoa *et al.* (1998) are able to do formal stability analysis on circular rodons, we are restricted to normal mode stability analysis. Andrews (1984) has shown that all solutions to the stability condition obtained from conservation integrals must have the same symmetries as the system does. Of course, there may well be (see examples in Ripa 1992) stable non-symmetrical solutions, but they cannot be found by means of formal analysis.

We now write the dependent variables as a basic state and a perturbation:

$$u_* = u_0 + U\,\mathrm{e}^{-\mathrm{i}\omega t}\epsilon + O(\epsilon^2), \tag{3.4}$$

$$v_* = v_0 + V\,\mathrm{e}^{-\mathrm{i}\omega t}\epsilon + O(\epsilon^2), \tag{3.5}$$

$$\phi = \phi_0 + \Phi\,\mathrm{e}^{-\mathrm{i}\omega t}\epsilon + O(\epsilon^2), \tag{3.6}$$

$$\psi = \psi_0 + \Psi\,\mathrm{e}^{-\mathrm{i}\omega t}\epsilon + O(\epsilon^2), \tag{3.7}$$

where U, V, Φ, Ψ depend on (x_*, y_*). As perturbations are proportional to $\mathrm{e}^{-\mathrm{i}\omega t}$, the linear instability criterion is

$$\mathrm{Im}\,(\omega) > 0.$$

When substituting into (2.6) we have, to $O(\epsilon)$, four equations for variables (U, V, Φ, Ψ):

$$-\mathrm{i}abU\omega M = -a^3b^3\frac{\partial \Phi}{\partial x_*}\hat{g}^{1/2} - a^2V\Omega_* M + abVf_* M$$
$$-a^2b^4\Omega_* f_*\hat{g}^{1/2}\Psi x_* + b^2\Omega_*\frac{\partial U}{\partial y_*}Mx_* - a^2\Omega_*\frac{\partial U}{\partial x_*}My_*, \qquad (3.8a)$$

$$-\mathrm{i}abV\omega M = -a^3b^3\frac{\partial \Psi}{\partial y_*}\hat{g}^{1/2} + b^2U\Omega_* M - abUf_* M$$
$$+b^2\Omega_*\frac{\partial V}{\partial y_*}Mx_* - a^4b^2\Omega_* f_*\hat{g}^{1/2}\Psi y_* - a^2\Omega_*\frac{\partial V}{\partial x_*}My_*, \qquad (3.8b)$$

$$-4\mathrm{i}a^3b^3\hat{g}^{1/2}\omega\Phi = -a^4b^4\Omega_*\frac{\partial U}{\partial x_*}f_* - a^4b^4\Omega_*\frac{\partial V}{\partial y_*}f_* - a^2b^2\Omega_*\frac{\partial U}{\partial x_*}f_* M$$
$$-a^2b^2\Omega_*\frac{\partial V}{\partial y_*}f_* M + 4a^2b^4\Omega_*\frac{\partial \Psi}{\partial y_*}\hat{g}^{1/2}x_* + 4b^2U\Omega_* f_* Mx_*$$
$$+a^2b^4\Omega_*\frac{\partial U}{\partial x_*}f_* x_*^2 + a^2b^4\Omega_*\frac{\partial V}{\partial y_*}f_* x_*^2 + b^2\Omega_*\frac{\partial U}{\partial x_*}f_* Mx_*^2$$
$$+b^2\Omega_*\frac{\partial V}{\partial y_*}f_* Mx_*^2 - 4a^4b^2\Omega_*\frac{\partial \Phi}{\partial x_*}\hat{g}^{1/2}y_* + 4a^2V\Omega_* f_* My_*$$
$$+a^4b^2\Omega_*\frac{\partial U}{\partial x_*}f_* y_*^2 + a^4b^2\Omega_*\frac{\partial V}{\partial y_*}f_* y_*^2 + a^2\Omega_*\frac{\partial U}{\partial x_*}f_* My_*^2$$
$$+a^2\Omega_*\frac{\partial V}{\partial y_*}f_* My_*^2, \qquad (3.8c)$$

$$-\mathrm{i}a^2b^2\hat{g}^{1/2}\Psi\omega = ab^3\Omega_*\frac{\partial \Psi}{\partial y_*}\hat{g}^{1/2}x_* - a^3b\Omega_*\frac{\partial \Psi}{\partial x_*}\hat{g}^{1/2}y_*$$
$$-\frac{2b^2U(a^2b^2 - M)x_*}{a^2b^2 - b^2x_*^2 - a^2y_*^2} - \frac{2a^2V(a^2b^2 - M)y_*}{a^2b^2 - b^2x_*^2 - a^2y_*^2}, \qquad (3.8d)$$

where $M = (a^2b^2 + \mu(a^2b^2 - b^2x_*^2 - a^2y_*^2))$.

We then apply a set of transformations (cf. Ripa 1987) in order to write the solutions to the system as a polynomial series in the independent variables

$$z = x_*/a + \mathrm{i}y_*/b, \qquad z_c = x_*/a - \mathrm{i}y_*/b, \qquad (3.9)$$

where the subscript c denotes complex conjugate. The variables U, V, Φ, Ψ are represented by A, B, C, D by means of

$$U = \mathrm{i}a(A + B), \qquad V = b(A - B), \qquad (3.10a)$$

$$\Phi = \frac{abf_* C}{\hat{g}^{1/2}}, \qquad \Psi = \frac{D}{\Omega_*\hat{g}^{1/2}}. \qquad (3.10b)$$

Finally, the system is turned around to separate variables A and B. If S_1 and S_2 are

the left-hand parts of (3.8*a*) and (3.8*b*), respectively, equations

$$bS_1 + \mathrm{i}aS_2 = 0, \tag{3.11a}$$

$$\mathrm{i}bS_1 + aS_2 = 0, \tag{3.11b}$$

will replace them in the system.

If S_3 and S_4 now represent the left-hand parts, respectively, of (3.8*c*) and (3.8*d*), a new system will result comprising (3.11*a*, *b*) and the two following equations:

$$S_3 = 0, \tag{3.11c}$$

$$S_4 = 0. \tag{3.11d}$$

In the new variables, we have

$$\begin{aligned} &A + \frac{\partial A}{\partial z}z - \frac{\partial A}{\partial z_c}z_c + \mu\left(-A - \frac{\partial A}{\partial z}z + \frac{\partial A}{\partial z_c}z_c\right)(-1 + z\,z_c) \\ &\quad + \frac{A\omega}{\Omega_*}(1 + \mu - \mu z\,z_c) + \frac{\alpha}{2}\left(-2A + 2\frac{\partial C}{\partial z_c} - 2A\mu + Dz + 2A\mu z\,z_c\right) \\ &\quad + \frac{\delta}{2}\left(2B + 2\frac{\partial C}{\partial z} + 2B\mu + Dz_c - 2B\mu z\,z_c\right) = 0, \end{aligned} \tag{3.12}$$

$$\begin{aligned} &-B + \frac{\partial B}{\partial z}z - \frac{\partial B}{\partial z_c}z_c + \mu\left(B - \frac{\partial B}{\partial z}z + \frac{\partial B}{\partial z_c}z_c\right)(-1 + z\,z_c) \\ &\quad + \frac{B\omega}{\Omega_*}(1 + \mu - \mu z\,z_c) + \frac{\delta}{2}\left(-2A + 2\frac{\partial C}{\partial z_c} - 2A\mu + Dz + 2A\mu z\,z_c\right) \\ &\quad + \frac{\alpha}{2}\left(2B + 2\frac{\partial C}{\partial z} + 2B\mu + Dz_c - 2B\mu z\,z_c\right) = 0, \end{aligned} \tag{3.13}$$

$$\begin{aligned} &-2\frac{\partial A}{\partial z} - 2\frac{\partial B}{\partial z_c} + 2C\frac{\omega}{\Omega_*} + 2Bz + 2\frac{\partial C}{\partial z}z + 2Az_c - 2\frac{\partial C}{\partial z_c}z_c + 2\frac{\partial A}{\partial z}z\,z_c + 2\frac{\partial B}{\partial z_c}z\,z_c \\ &\quad + \mu(-1 + z\,z_c)\left(\frac{\partial A}{\partial z} + \frac{\partial B}{\partial z_c} - 2Bz - 2Az_c - \frac{\partial A}{\partial z}z\,z_c - \frac{\partial B}{\partial z_c}z\,z_c\right) = 0, \end{aligned} \tag{3.14}$$

$$D\frac{\omega}{\Omega_*} + \frac{\partial D}{\partial z}z - \frac{\partial D}{\partial z_c}z_c + 2\mu(Bz + Az_c) = 0. \tag{3.15}$$

We now write the functions A, B, C, D as polynomials in z, z_c:

$$A = \sum_{m=0}^{n-1}\sum_{s=0}^{m} A_{ms} z^{m-s} z_c^s, \tag{3.16a}$$

$$B = \sum_{m=0}^{n-1}\sum_{s=0}^{m} B_{ms} z^{m-s} z_c^s, \tag{3.16b}$$

$$C = \sum_{m=0}^{n}\sum_{s=0}^{m} C_{ms} z^{m-s} z_c^s, \tag{3.16c}$$

$$D = \sum_{m=0}^{n-2}\sum_{s=0}^{m} D_{ms} z^{m-s} z_c^s. \tag{3.16d}$$

As in Ripa (1987), n is called the polynomial degree of system (3.16), with the limits indicated by the defining equations. Each power-combination term of $z\, z_c$ is linearly independent of the rest. Thus we obtain an equation set for every polynomial degree.

4. Results

4.1. *Polynomial degree-1 set*

The simplest non-trivial system obtained from (3.16), namely for $n = 1$, is used to calculate C_{00}, B_{00}, A_{00}, C_{10} and C_{11}. The system matrix is

$$\begin{pmatrix} 0 & 0 & 0 & 0 & 0 \\ 0 & 1-\alpha & \delta & -\alpha/(1+\mu) & -\delta/(1+\mu) \\ 0 & -\delta & -1+\alpha & -\delta/(1+\mu) & -\alpha/(1+\mu) \\ 0 & -1-\mu & 0 & -1 & 0 \\ 0 & 0 & -1-\mu & 0 & 1 \end{pmatrix}, \tag{4.1}$$

where

$$\alpha = \frac{f_*}{2\Omega_*}\left(\frac{b}{a} + \frac{a}{b}\right), \tag{4.2}$$

$$\delta = \frac{f_*}{2\Omega_*}\left(\frac{b}{a} - \frac{a}{b}\right). \tag{4.3}$$

Its characteristic polynomial,

$$-\omega + (2 + \alpha^2 - \delta^2)\omega^3 - \omega^5 = 0,$$

is simple enough to have its non-zero roots expressed analytically:

$$\omega = \pm(\tfrac{1}{2})^{1/2}\left(2 + \alpha^2 - \delta^2 \pm (4\alpha^2 + \alpha^4 - 4\delta^2 - 2\alpha^2\delta^2 + \delta^4)^{1/2}\right)^{1/2}. \tag{4.4}$$

The parameter μ is not yet present in the eigenvalue calculations, but it will appear in higher-degree polynomials (Pinet 1998). For $n = 1$ all eigenvalues are real: there are no unstable components.

4.2. *Polynomial degrees 2–5*

The degree-2 characteristic polynomial is considerably more complicated:

$$\begin{aligned} &(-16 - 4\alpha^3 - \alpha^4 + 8\delta^2 - \delta^4 + \alpha^2(-8 + 2\delta^2) + \alpha(-16 + 4\delta^2))\omega^5 \\ &\quad + (40 + 4\alpha^5 + \alpha^6 - 34\delta^2 + 10\delta^4 - \delta^6 + \alpha^3(24 - 8\delta^2) + \alpha^4(10 - 3\delta^2) \\ &\quad + \alpha^2(34 - 20\delta^2 + 3\delta^4) + \alpha(36 - 24\delta^2 + 4\delta^4))\omega^7 \\ &\quad + (-33 - 8\alpha^3 - 3\alpha^4 + 20\delta^2 - 3\delta^4 + \alpha^2(-20 + 6\delta^2) + \alpha(-24 + 8\delta^2))\omega^9 \\ &\quad + (10 + 4\alpha + 3\alpha^2 - 3\delta^2)\omega^{11} - \omega^{13} = 0. \end{aligned} \tag{4.5}$$

It also has eigenvalues with null imaginary parts for the ranges considered ($0 \leqslant a/b \leqslant 1, 0 \leqslant \Omega/f \leqslant 0.5$). Non-zero eigenvalues for the polynomial degree-2 system are

$$\pm(4 + \alpha^2 - \delta^2)^{1/2},$$

$$\pm(4 + 4\alpha + \alpha^2 - \delta^2)^{1/2},$$

$$\pm\frac{1}{\sqrt{2}}\left(2 + \alpha^2 - \delta^2 \pm (4\alpha^2 + \alpha^4 - 4\delta^2 - 2\alpha^2\delta^2 + \delta^4)^{1/2}\right)^{1/2}.$$

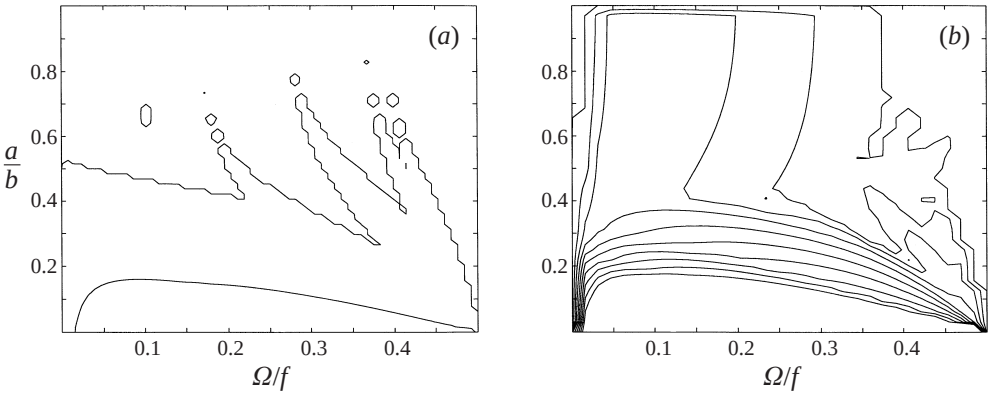

FIGURE 1. Effect of density inhomogeneity on the stability of an elliptical rodon. (*a*) The stability diagram for polynomial degree-5 perturbations to a base rodon with $\mu = 0$; (*b*) is for $\mu = -0.04$. Contours are for perturbation growth (Im(ω)) in Ω_* units: in (*a*) they are 0.0 and 1.0; and in (*b*), 0.0 to 1.0 in 0.1 intervals.

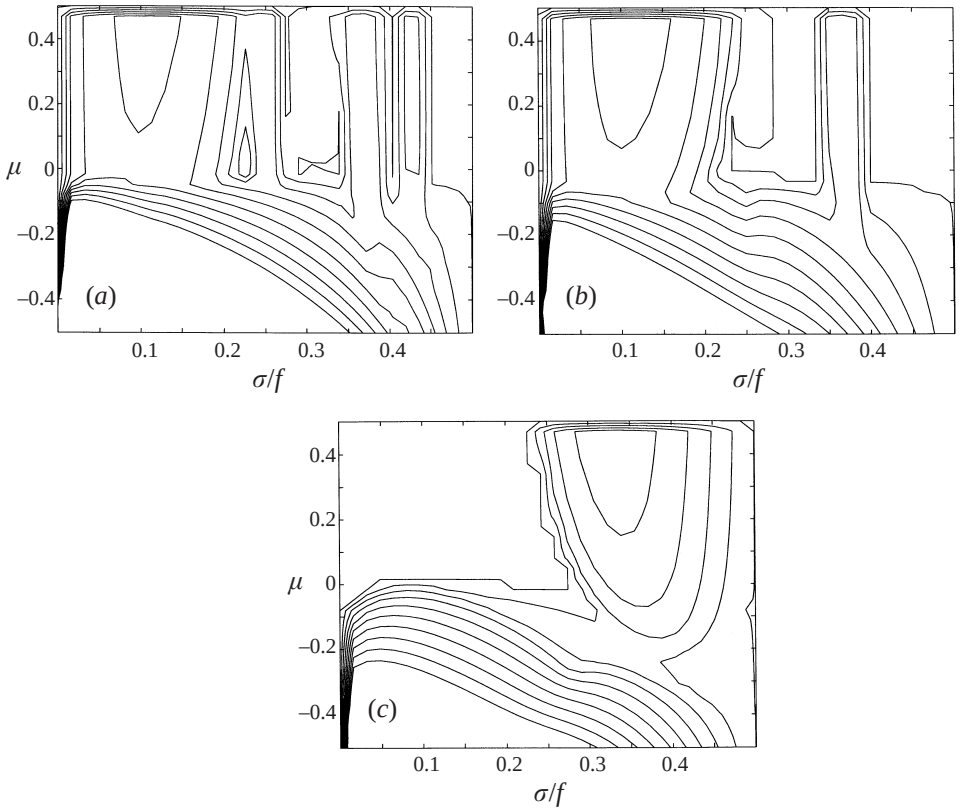

FIGURE 2. Contours 0.0–1.0 of growth rate for a polynomial degree-5 perturbation to an inhomogeneous elliptical vortex ($a/b = 0.4$). There are unstable solutions even for $\mu > 0$. Contour increment is $0.05\,\Omega_*$. (*b*, *c*) As (*a*) but for degree 4 and 3 respectively.

As in the homogeneous case, eigenvalues for polynomial degrees 0, 1 and 2 of the inhomogeneous problem are all real. However, at polynomial degrees 3, 4 and 5 there are zones in the stability diagrams that indicate imaginary parts greater than zero for the eigenvalues.

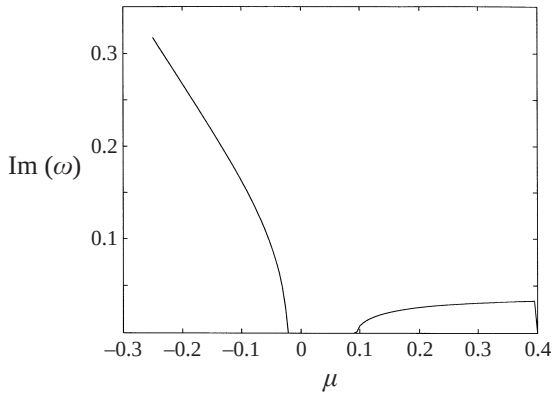

FIGURE 3. Growth rate (in Ω_* units), of a polynomial-degree-4 perturbation to an inhomogeneous ($\Omega/f = 0.25$), elliptical ($a/b = 0.5$) vortex.

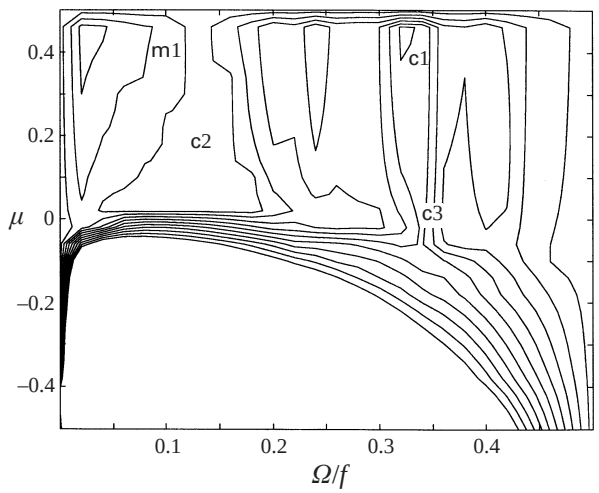

FIGURE 4. Location of initial states for some numerical experiments in the stability diagram for polynomial degree 3, 4 and 5 perturbations to an inhomogeneous elliptic (aspect ratio $a/b = 0.5$) rodon.The experiments refer to figures 5 and 6. Only 0.05-step contours between 0.05 and 2.0 are shown for $\mathrm{Im}(\omega)/\Omega_*$.

We calculated eigenvalues for polynomial perturbations, up to degree 5, to inhomogeneous elliptical vortices. Figure 1 shows, for instance, the effect of the inhomogeneity parameter μ. Part (a) is a diagram similar to figure 7 in Ripa (1987); they are not exactly equivalent because density perturbations have been allowed in our case. These stability diagrams have been extended to include inhomogeneous rodons.

Figure 2(a) shows, as another example, maxima values reached by the imaginary part of the eigenvalues associated with a degree-5 polynomial perturbation. They have been calculated for an $a/b = 0.4$ rodon. Unstable normal modes appear even for positive values of the inhomogeneity parameter μ. Therefore, the formal stability criterion ($\mu > 0$) cannot be extended from circular vortices to elliptical ones. Figures 2(b) and 2(c) show the corresponding contours for polynomial degrees 4 and 3.

Figure 3 demonstrates a further point: we compute the maximum imaginary component of all the eigenvalues of degree-4 polynomial perturbations to ellip-

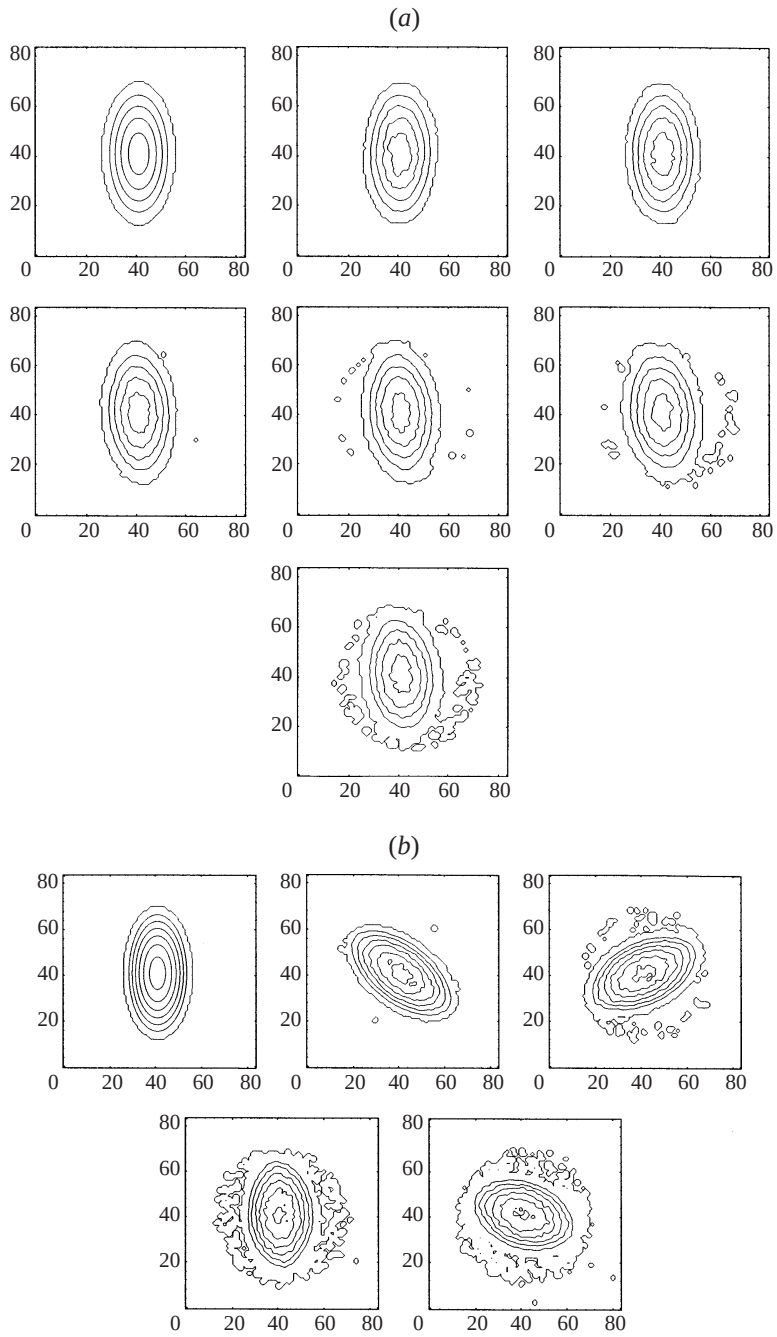

FIGURE 5. Depth contours for numerical experiments m1 (*a*) and c2 (*b*). Initial states for both simulations are in the 'neutral stability' zones of the stability diagram. If these eddies were located at 30° latitude, the spacing between frames would be somewhat less than a week.

tical inhomogeneous vortices (parameters are $\Omega/f = 0.25$, and $a/b = 0.5$). The inhomogeneity parameter μ ranges along the horizontal axis from $-\frac{1}{4}$ to near $\frac{1}{2}$. On both sides, at least one eigenvalue bifurcates giving rise to an unstable response. However, this happens at a finite distance from the line $\mu = 0$. A perturbation analysis

taking an homogeneous rodon ($\mu = 0$) as base solution would not detect any of these bifurcations.

4.3. *Numerical simulations*

The details of the numerical model are given in Ochoa *et al.* (1998). It is a particle-in-cell simulation (cf. Pavía & Cushman-Roisin 1988) producing the Lagrangian positions of fluid column particles from an Eulerian velocity field at different time steps, and from these the Eulerian velocity field is recalculated. From these results, density distribution and interface layer depth – among many other variables – can be calculated.

Figure 4 is a stability diagram formed by the superposition of growth rate contour levels for polynomial perturbations of degrees 3, 4 and 5, calculated for inhomogeneous rodons with aspect ratio $a/b = 0.5$. On it, initial states of several numerical simulations are located. Their evolutions are observed in the sequences shown in figures 5 and 6. While in the analytical treatment perturbations can be classified by polynomial degree and analysed accordingly, no such refinement is possible in the numerical simulation, i.e. the perturbations are given by the random computational process. We used 18 019 particles in the simulations, and considered the eddy border to be the contour line corresponding to 1/1000 th of the maximum interface depth.

The experiments referred to as m1 and c2 are shown in figure 5. These initial states are close to the 'neutral stability' line, while experiments c1 and c3, shown in figure 6, have their initial states in more unstable zones of the diagram; their change is more noticeable and much faster. Note also that unstable eddies increase their aspect ratio and shed mass, particularly noticeable in figure 6.

If calculations were carried out at 30° latitude, the time-lapse between frames in the former simulations would be 6.25 days for m1, and 6.9 days for c2, while frames in the latter two would be separated by 36.1 hours for c1, and 17.6 hours for c3.

5. Discussion

If the effect of variable density is ignored in equations (3.8*a–d*), on setting $\mu = 0$ and $D_{mn} = 0\ \forall\, m, n$, the stability diagrams become those of Ripa (1987).

5.1. *Thermal wind*

In order to estimate the validity of a model by means of comparison with a better-resolution alternative, Ripa (1995) introduced a series of models based on the primitive equations. The models using vertical averages in velocity, pressure gradients and density distribution were called L^0. The models approximating vertical dependence by a linear function $u(x, \sigma, t) = \bar{u}(x, t) + \sigma u_\sigma(x, t)$, were called L^1. Here σ is a vertical coordinate mapping the range $\{z | z \in [0, h]\}$ to the interval $\{\sigma | \sigma \in [-1, 1]\}$. That is,

$$z = h(1 - \sigma)/2, \tag{5.1}$$

where h is the layer's depth, and so forth: a model representing vertical dependence by a n-degree polynomial is called 'the L^n approximation'.†

Ripa then compared baroclinic instability predictions from models L^0 and L^1, using a parallel-flow scheme $\boldsymbol{u} = \overline{U}\hat{\boldsymbol{x}}$, and obtaining critical wavenumbers as functions of

† Or rather $\mathrm{IL}^n\mathrm{PE}$ for 'Inhomogeneous Layer Primitive Equations (Model)'.

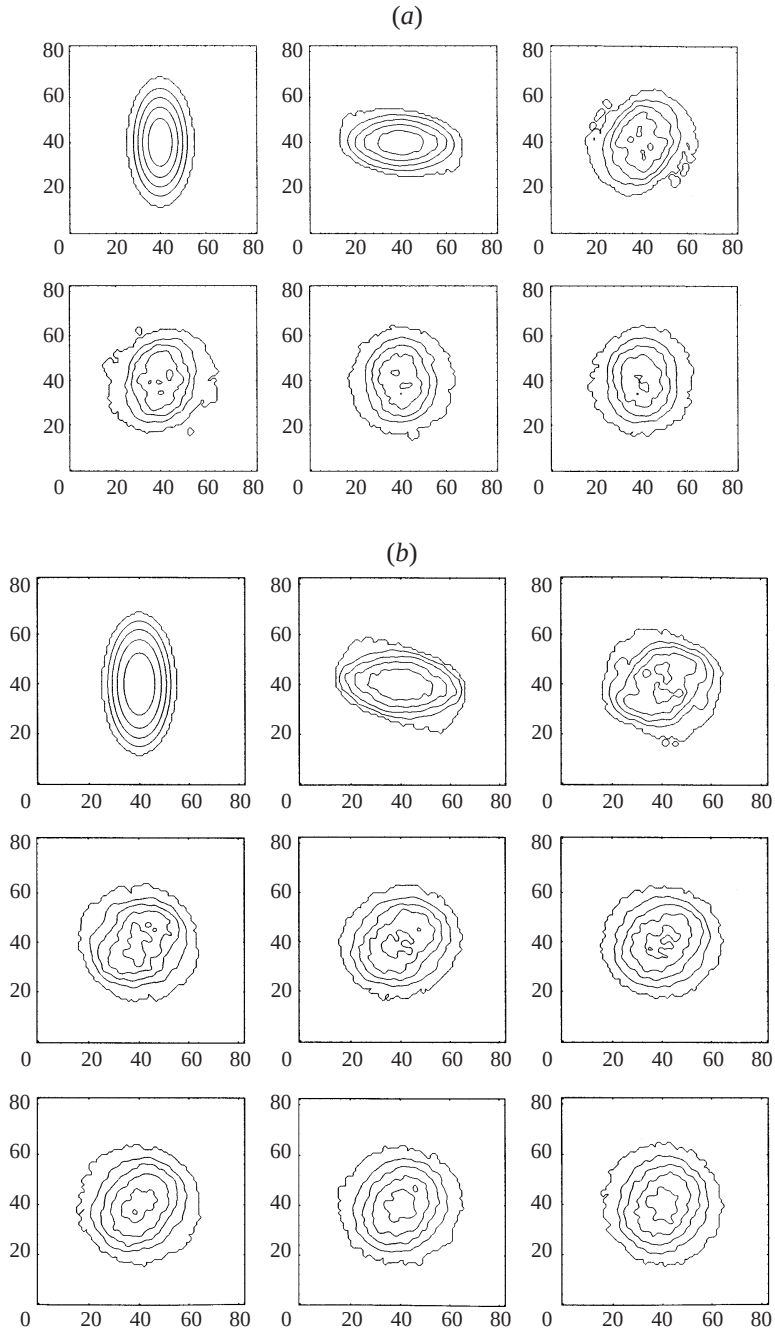

FIGURE 6. Depth contours for numerical experiments c1 (*a*) and c3 (*b*). Initial states for both simulations are in the 'instability' zones of the stability diagram. If these eddies were located at 30° latitude, the spacing between frames would be somewhat less than a day.

$\overline{U}/U_\sigma$, where $U_\sigma = \partial\overline{U}/\partial\sigma$. For the L^0 case, Ripa considered U_σ implicitly defined so as to satisfy the thermal wind equation

$$U_\sigma = -\frac{h_0}{2f}\theta_0'(y). \tag{5.2}$$

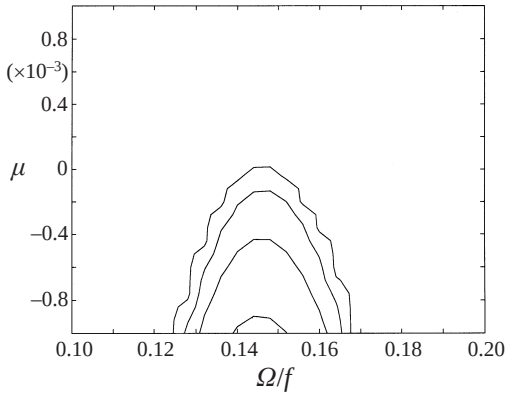

FIGURE 7. Growth rate $\mathrm{Im}(\omega)/f$ for a narrow band ($10^{-3} < \mu < 10^{3}$) in the stability diagram for inhomogeneous circular rodons. The figure is consistent with the formal analysis stability criterion ($\mu > 0$) as a necessary, not a suficcient, condition.

$\mathrm{IL}^0\mathrm{PE}$ fails to detect growing perturbations shown by $\mathrm{IL}^1\mathrm{PE}$ for the range $\overline{U}/U_\sigma < 0$. However, for $\overline{U}/U_\sigma > 0$, $\mathrm{IL}^0\mathrm{PE}$ predictions are very similar to those of $\mathrm{IL}^1\mathrm{PE}$ – and, even, to those of the two-layer model. For the range $\overline{U}/U_\sigma > 0$, in this sense, predictions made with $\mathrm{IL}^1\mathrm{PE}$ are valid.

A similar verification specifically for circular vortices is still underway; nevertheless we can obtain values of $\overline{U}/U_\sigma$ from the thermal wind equation. In the remainder of this section we will again use polar components for $\boldsymbol{u} = (u, v)$. That is,

$$\begin{cases} u: & \text{radial velocity component,} \\ v: & \text{azimuthal velocity component.} \end{cases}$$

The thermal wind equation is easily obtained for circular rodons. These are axisymmetric functions, solid-body rotating at angular speed Ω:

$$\phi = \phi_0(\hat{h}), \quad \boldsymbol{u} = (0, -\Omega r), \quad \gamma = \gamma_0(\hat{h}). \tag{5.3}$$

Upon substitution in equations (1.1), (1.1*a*) and (1.1*c*) become trivially satisfied, while (1.1*b*) results in

$$f\Omega r - \Omega^2 r + \gamma_0 \phi_0' = 0, \tag{5.4}$$

and the equations of motion are

$$-\frac{v^2}{r} - fv + \frac{1}{\bar{\rho}}\frac{\partial p}{\partial r} = 0, \quad \frac{\partial p}{\partial z} = -\rho g. \tag{5.5}$$

The velocity vertical shear, from (5.5) and (5.1) results in

$$v_\sigma = \frac{h\theta'(r)}{4\Omega_* - 2f}, \tag{5.6}$$

so that

$$\frac{v}{v_\sigma} = -\frac{\Omega_*(4\Omega_* - 2f)r}{\theta'(r)h}. \tag{5.7}$$

For the solution (2.9) from Ochoa *et al.* (1998)

$$\theta'(r) = \frac{2\gamma_0 \mu r}{(1 + \mu(1 - \hat{h}))^2}. \tag{5.8}$$

Equation 5.7 becomes

$$\frac{v}{v_\sigma} = 4G(\Omega/f)\frac{\mu\hat{h} - \mu - 1}{\mu(\hat{h} - 1)(\mu\hat{h} - \mu - 2)}, \tag{5.9}$$

where

$$G(\Omega/f) = \frac{2((1 - \Omega/f)\Omega/f)^{1/2} - 1}{(\Omega/f)(2\Omega/f - 1)}\left((1 - \Omega/f)\Omega/f\right)^{1/2}.$$

For the range used in this paper ($0 \leqslant \Omega/f < 0.5$), $G(\Omega/f)$ is defined and positive. We can see from (5.9) that positive values of v/v_σ are associated with negative values of μ, and vice versa.

6. Conclusions

The stability criterion obtained from formal analysis for inhomogeneous circular rodons (density must increase towards the centre) cannot be extended to elliptical vortices. We use normal mode analysis to show examples of vortices satisfying the stability condition and yet they are unstable. Figure 7 is an indication that, even for circular rodons, the criterion is necessary but not sufficient.

The parameters determining the system stability (rotation speed Ω/f, aspect ratio a/b and density inhomogeneity μ) have instability zones in the diagram at finite distances from their axes (see e.g. figure 3). Therefore, a perturbation analysis for *these parameters* (as, for instance, in Maas & Zahariev 1996) would fail to show them.

In all numerically analysed cases, the instability implied loss of mass to the surroundings and an increase in aspect ratio, or axisymmetrization, a behaviour reported by Pavía & López (1994) for homogeneous vortices.

Finally we notice that one could divide the instabilities of inhomogeneous elliptical vortices into two kinds: 'baroclinic' and 'geometrical'. The former, which produces homogeneization of density, is due to the concealed vertical shear implied in the horizontal density gradients; and the latter, which produces shedding of mass and axisymmetrization, is due to the vortex eccentricity and intensity.

The authors would like to express their gratitude to Drs Pedro Ripa, Julio Sheinbaum, Affonso Mascarenhas, Javier Berón Vera, and Héctor Echavarría for comments and corrections; and to CONACYT (grants 4919E and 28794T) and ANUIES (Mexican governmental agencies) for financial support.

REFERENCES

Andrews, D. 1984 On the existence of nonzonal flows satisfying sufficient conditions for stability. *Geophys. Astrophys. Fluid Dyn.* **28**, 243–256.

Holm, D. D., Marsden, J. E., Ratiu, T. & Weinstein, A. 1985 Nonlinear stability of fluid and plasma equilibria. *Phys. Rep.* **123**, 1–116.

Maas, L. R. M. & Zahariev, K. 1996 An exact, stratified model of a meddy. *Dyn. Atmos. Oceans* **24**, 215–225.

Ochoa, J., Sheinbaum, J. & Pavía, E. 1998 Inhomogeneous rodons. *J. Geophys. Res.* **103**, 24869–24880.

Pavía, E. G. & Cushman-Roisin, B. 1988 Modeling of oceanic fronts using a particle method. *J. Geophys. Res.* **93**, 3554–3562.

Pavía, E. G. & López, M. 1994 Long-term evolution of elongated warm eddies. *J. Phys. Oceanogr.* **24**, 2201–2208.

PINET, R. 1998 Estabilidad de remolinos inhomogéneos elípticos. PhD thesis, Facultad de Ciencias Marinas, Universidad Autónoma de Baja California.

RIPA, P. 1987 On the stability of elliptical vortex solutions of the shallow-water equations. *J. Fluid Mech.* **183**, 343–363.

RIPA, P. 1992 A tale of three theorems. *Revista Mexicana de Física* **38**, 229–243.

RIPA, P. 1995 On improving a one-layer ocean model with thermodynamics. *J. Fluid Mech.* **303**, 169–201.

RIPA, P. 1996 Linear waves in a one-layer ocean model with thermodynamics. *J. Geophys. Res.* **101**, 1233–1245.

SCHOPF, P. & CANE, M. 1983 On equatorial dynamics, mixed layer physics and sea surface temperature. *J. Phys. Oceanogr.* **13**, 917–935.